GDF11 MEDIATES CARDIAC AND SKELETAL MUSCLE DYSFUNCTION AND CACHEXIA

Tiffany Liang

Submitted to the faculty of the University Graduate School
in partial fulfillment of the requirements
for the degree
Master of Science
in the Translational Science Program,
Indiana University

August 2016

Accepted by the Graduate Faculty, Indiana University, in partial fulfillment of the requirements for the degree of Master of Science.

Master's Thesis Committee

_____
Leonidas G. Koniaris, MD, Chair

_____
Teresa A. Zimmers, PhD

_____
Michael P. Murphy, MD

ACKNOWLEDGEMENTS

Leonidas G. Koniaris, MD, FACS

Teresa A. Zimmers, PhD

Michael P. Murphy, MD

Yanlin Jiang, MD

Meijing Wang, MD

Joseph E. Rupert

Ernie D. Au

Jianguo Liu

Tiffany Liang

GDF11 MEDIATES CARDIAC AND SKELETAL MUSCLE DYSFUNCTION AND CACHEXIA

Growth differentiation factor 11 (GDF11) is important in regulating early fetal development of the axial skeleton and various visceral organs. Its actions on the adult body are less clear, and recent studies have led to conflicting accounts of GDF11's ability to affect cardiac hypertrophy and skeletal muscle regeneration. If boosting GDF11 levels in adults had the ability to rejuvenate tissues and reverse the effects of aging, then the therapeutic possibilities are potentially vast. We attempted to provide clarification of this controversial topic by studying the effects of supraphysiologic levels of GDF11 in a mouse model using injected Chinese hamster ovary cells producing GDF11. We found that increasing endogenous levels of GDF11 in this *in vivo* mouse model resulted in overall bodily wasting, specifically with evidence of cardiac and skeletal muscle atrophy. In light of these results, caution must be exercised if GDF11 is ever considered as a potential therapeutic agent.

Leonidas G. Koniaris, MD, Chair

TABLE OF CONTENTS

LIST OF FIGURES

LIST OF ABBREVIATIONS

CHO ..... Chinese hamster ovary

CSA ..... Cross-sectional area

ECG ..... Electrocardiography

GDF11 ..... Growth differentiation factor 11

GDF8 ..... Growth differentiation factor 8

MAFbx ..... Muscle atrophy F-box

INTRODUCTION/BACKGROUND

Growth differentiation factor 11 (GDF11) is a member of the transforming growth factor-beta superfamily of growth factors and highly homologous to myostatin/GDF8 (Nakashima et al., 1999). GDF11 was first described in the literature as a secreted factor involved in tooth development (Nakashima et al., 1999), as well as axial patterning and renal genesis (McPherron et al., 1999).

More recently, work in adult mouse tissue reported a muscle regenerative potential for GDF11, with some describing it as “factor of youth” since it declined with age, and exogenous dosing was responsible for both reversing cardiac hypertrophy as well as improving skeletal muscle structure and function in aged animals (Andersen and Lim, 2014; Loffredo et al., 2013; Sinha et al., 2014). Subsequent research questioned these initial conclusions, with disagreements regarding the validity of the reagents and assays used in the experimental procedures as well as the interpretation of the results (Egerman et al., 2015; Poggioli et al., 2016; Rodgers and Eldridge, 2015). Additionally, further research into the effects of GDF11 on the hearts of aged mice did not find a regenerative potential, contrary to previous reports (Smith et al., 2015).

Understanding the *in vivo* effects of secreted proteins remains difficult due to problems related to administration, bioavailability and dosing. These difficulties have limited the development of an understanding of the role of GDF11 *in vivo* and likely have increased the controversy surrounding its activities due to the fact that many experiments to date did not directly examine *in vivo* actions. Very successful determination of *in vivo* activities of secreted factors has been obtained utilizing cells that secrete active protein, as this allows sustained and high levels of *in vivo* expression. Using such an approach, we have identified *in vivo* effects for various other secreted factors including IL-6 and myostatin (Bonetto et al., 2012; Jin et al., 2007; Jin et al., 2006; Zimmers et al., 2002; Zimmers et al., 2003). Herein, we sought to look at the

systemic effects of GDF11 *in vivo* by using a Chinese hamster ovary (CHO) cell overexpression model to determine *in vivo* effects of this controversial, but critical growth and differentiation factor.

RESEARCH DESIGN

Mice

Male athymic nu/nu mice were obtained from Harlan Laboratories, Inc. (Indianapolis, IN, USA). For GDF11 administration, a CHO cell line stably producing GDF11 (CHO-GDF11) was obtained by introduction of the plasmid vector pMSXND containing full-length *Gdf11* cDNA into DHFR-deficient CHO-DUXX cells by protoplast fusion and subsequent methotrexate selection. A similarly selected CHO cell line (CHO-control) not expressing detectable recombinant protein was used as a control. 10-week old mice were placed under isoflurane general anesthesia using a non-rebreathing apparatus on a heated re-circulating waterbed, and then intramuscularly injected in the upper rear portion of the right hind limbs with either 5×10^5 CHO-GDF11 cells per mouse or 5×10^3 CHO-control cells in 0.1 mL of PBS. Total body weight was obtained daily until euthanasia. Tumor size was measured at intervals and at euthanasia. One mouse in the GDF11 group did not grow appreciable tumor, so the data obtained from this mouse was not included in subsequent analyses. At 10 and 13 days after CHO cell injection, euthanasia was performed under isoflurane anesthesia by exanguination through cardiac puncture followed by cervical dislocation and tissue collection. Muscles of the left hind limb as well as hearts were collected and weighed, then either snap frozen with liquid nitrogen or embedded in Tissue-Tek® OCT compound (Sakura Finetek USA, Inc., Torrance, CA, USA) and snap frozen in isopentane, and then stored in −80°C for later processing. Other organs and the carcass were also collected and weighed. Left tibia length was measured. All experiments were approved by and performed according to the guidelines of the Institutional Animal Care and Use Committees at Indiana University School of Medicine.

Echocardiography

Cardiac muscle dimensions and function were assessed at 8, 10, and 13 days after CHO cell injection via echocardiography using the Vevo® 2100 system (Fujifilm VisualSonics Inc., Toronto, Canada). Mice were placed under isoflurane anesthesia for the duration of the procedure, adjusting the level to maintain a heart rate of 400 – 500 beats per minute. Left ventricular dimensions and function were assessed by M-mode scanning of the left ventricular chamber.

Electrocardiography

Electrocardiogram (ECG) recordings were taken at 7, 9, and 13 days after CHO cell injection using the ECGenie apparatus (Mouse Specifics, Inc., Boston, MA, USA) as previously described (Mielcarek et al., 2014). Conscious mice were placed on a platform with footplate electrodes that captured a signal that is transduced to electrical voltage, as represented on the ECG recording. Several minutes of recording were obtained, and selected 1 – 5 second recordings of PQRST complexes were analyzed for various intervals using the eMouse signal analysis software (Mouse Specifics, Inc., Boston, MA, USA). Heart rate and heart rate variability were also obtained via this software.

Body composition analysis

Lean and whole body fat masses were measured at 9 and 13 days after CHO cell injection using EchoMRI™ (Echo Medical Systems, Houston, TX, USA). Conscious mice were immobilized by placement in a cylindrical apparatus, and then body composition was analyzed with the EchoMRI™ machine. Two measurements were taken per mouse per analysis and averaged to determine the final data point.

Grip strength measurement

Grip strength was determined at 10 and 13 days after CHO cell injection using a force gauge (Extech Instruments, Nashua, NH, USA). The mice were grasped at the base of the tail and lifted onto a metal grid. Once all four feet gripped the grid, they were

pulled backward by the base of the tail until they released their grip. Three measurements were taken in this fashion at each time point.

Gene expression studies

qRT-PCR was used to measure the mRNA expression levels of *atrogin-1*, *MuRF1*, *Pax 7*, *Mki67*, *Bnip3*, *Bnip3L*, *Myh6*, *Myh7*, *Anp*, and *Bnp* in previously snap frozen mouse heart and quadriceps muscle. The total RNA was extracted using the Qiagen miRNeasy Mini kit (Valencia, CA) according to the manufacturer's instructions. The extracted RNA was quantified by NanoDrop (Thermo Scientific) at a wavelength of 260 nm, and the RNA integrity number was measured with Agilent RNA ScreenTape System (Agilent Technologies). cDNA was synthesized by Thermo Scientific Verso cDNA synthesis kit according to manufacturer's protocol. Primers were purchased from Life Technologies. qRT-PCR was conducted on a Roche LightCycler 96 Real-Time PCR System (Roche) using TaqMan Universal Master Mix II, with UNG (Life Technologies) in a 20 µl final reaction mixture. The cycling conditions were as follows: preincubation at 95°C for 1 min and 50 cycles of 10 s at 95 °C, and 1 min at 60 °C. Experiments were performed in triplicate for each sample. Results were normalized to either TBP or 18S, and fold difference was calculated by $2^{-\Delta\Delta Ct}$.

Western blot analysis

Snap frozen mouse heart and quadriceps muscle were homogenized in modified RIPA buffer. Protein was quantified using Pierce BCA protein assay kit (Thermo scientific, Rockford, IL). Tissue homogenates were separated by polyacrylamide gel (Bio-Rad) electrophoresis under reducing conditions. Proteins from the gels were electrophoretically transferred to Nitrocellulose membranes (Bio-Rad). Immunoblotting was performed using the following antibodies: LC3B (Sigma, Saint Louis, MO); p62 (BD Transduction Laboratories); pSMAD2, SMAD2, pAKT, AKT, pFOXO3a, FOXO3a, p4E-BP1 70, p4E-BP1 65, p4E-BP1 37/46, 4E-BP1, ubiquitin, and GAPDH (Cell Signaling

Technology). Antibody binding was detected following appropriate secondary antibody methods using SuperSignal West Femto (Thermo Scientific) or Odyssey CLx western blot detection system (Li-Cor, Lincoln, NE). Protein quantification was performed with ImageJ (NIH, Bethesda, MD, USA).

Histology and immunofluorescence

Hearts were snap frozen in isopentane cooled in liquid nitrogen immediately after sacrifice for histological analyses. Hearts were cut into 7 μm sections on a cryostat and mounted onto glass slides (Superfrost™ Plus Microscope Slides; Fisher Scientific), and stained with hematoxylin and eosin using standard procedures. Quantification of cardiomyocyte cross-sectional area (CSA) was measured manually using ImageJ (NIH, Bethesda, MD, USA). Measurements were obtained from ten, non-overlapping 20X fields from each cross-section per animal in each treatment group. A mean was then calculated for each animal from the CSA measurements recorded.

The tibialis muscle was excised immediately after sacrifice and snap frozen in isopentane cooled in liquid nitrogen. The tibialis was cut into 10 μm sections on a cryostat and mounted onto glass slides (Superfrost™ Plus Microscope Slides; Fisher Scientific). Tibialis sections were post-fixed in 4% paraformaldehyde (Affymetrix; Santa Clara, CA). Sections were blocked in 8% bovine serum albumin and reacted with an anti-dystrophin antibody (1:400, Vector Laboratories; Burlingame, CA) overnight at 4° C. Sections were washed and incubated with a fluorescent secondary antibody (1:1000, Alexa Fluor® 594; Fisher Scientific) for one hour at room temperature. Slide cover glass was mounted using aqueous mounting media. Sections were visualized using a fluorescent camera on an Observer.Z1 system (Zeiss; Oberkochen, Germany) and measurements were obtained from ten, non-overlapping 10X fields from each cross-section per animal in each treatment group using an Image J macro (Minamoto et al., 2007). Means were calculated from total CSA measurements for each individual animal.

Statistical analyses

Unpaired t-test or one-way analysis of variance with multiple comparisons were used to detect statistical significance with GraphPad Prism version 6.07 for Windows, GraphPad Software, La Jolla California USA, www.graphpad.com.

RESULTS

Overall Body Weight and Composition Decrease with GDF11 Overexpression

We first sought to characterize the global effects of GDF11 overexpression in adult male mice. Mice were divided into three groups – a normal group where no cells were injected, a control group where CHO cells expressing no recombinant protein were injected, and an experimental group where CHO cells overexpressing GDF11 were injected into the right hind limb. At day 10 after injection, the body weights of the GDF11 mice were significantly reduced compared to the control mice; this difference was even greater at day 13 (Figure 1A). A significant decrease in whole body lean mass as measured by EchoMRI™, however, was not seen until day 13, whereas there was no difference in whole body fat mass measured by EchoMRI™, between the groups (Figure 1B). Regardless, dramatic size differences in gross anatomy were seen at day 15 (Figures 1C and 1D). At necropsy, weights of various organs, such as the heart (Figures 1D, 2A and 2B), skeletal muscle (Figures 5A, 5B, and 5C), epididymal fat pad, kidney, and liver, as well as the carcasses (Figure S1) of the GDF11 mice were significantly decreased at day 13.

Heart Weight and Cardiomyocyte Size Decrease with GDF11 Overexpression

There are conflicting prior reports on the effect of GDF11 administration on mouse heart and cardiomyocyte size (Loffredo et al., 2013; Poggioli et al., 2016; Smith et al., 2015). Our studies using overexpression of GDF11 in mice showed that heart weight and cardiomyocyte size decreased significantly compared to controls by day 13 of GDF11 exposure, consistent with the Loffredo and Poggioli studies. Heart weights when normalized using both initial body weight (Figure 2A) and tibia length (Figure 2B) yielded similar results. The GDF11 group showed a significant weight reduction in cardiac mass by day 10 that was even more apparent by day 13. Mean cardiomyocyte cross-sectional area of the GDF11 group was significantly smaller than controls at day

13 (Figure 2C). Correspondingly, the frequency distribution of these area measurements demonstrated a left shift in the GDF11 group size distribution compared to controls (Figure 2D). Fresh mouse hearts and hematoxylin and eosin staining of histologic cross-sections of the heart through the left and right ventricles demonstrate visibly smaller heart and cardiomyocyte size in the GDF11 group (Figure 2E).

Gene Markers in Hearts of Mice with GDF11 Overexpression Indicate Muscle Atrophy

In addition to morphologic changes, the gene expression profile of hearts exposed to GDF11 differed from controls. In particular, the gene expression of ubiquitin-protein ligases atrogin-1, also known as muscle atrophy F-box (MAFbx), and MuRF1 (Bodine et al., 2001; Gomes et al., 2001) was increased at days 10 and 13, although the increase in *atrogin-1*/*MAFbx* at day 13 did not reach statistical significance (Figure 2F). Moreover, there was evidence of diminished cellular proliferation with the decreased expression of *Mki67* and autophagy with the increased expression of *Bnip3* in the GDF11 mice at day 13. Differences in *Bnip3L* expression were not statistically significant following GDF11 exposure (Figure 2F). This expression profile suggests activation of muscle atrophy pathways.

Expression of gene markers of cardiac dysfunction was generally unchanged with GDF11 overexpression compared to controls. Similar to results from a recent study examining the effects of GDF11 on mouse hearts (Smith et al., 2015), we did not find any statistically significant changes in the expression of *Anp*, *Myh6* (αMHC), or *Myh7* (βMHC) in the GDF11 group. While expression of *Bnp* at day 10 was significantly increased in the GDF11 group compared to control, the difference at day 13 did not reach statistical significance (Figure 2F).

Echocardiography in Mice with GDF11 Overexpression Demonstrates Reduced Cardiac Size and Function

Echocardiographic studies supported our findings that the hearts of mice with GDF11 overexpression are reduced in size compared to controls and further demonstrated a reduction in function. Parasternal long and short axis views captured in brightness mode (B-mode) ultrasound on day 13 after injection demonstrate that the GDF11 mice have decreased left ventricular size compared to controls (Figures 3A and 3B). Motion mode (M-mode) images on day 13 (Figure 3C) were used to measure cardiac dimensions and calculate functional assessments (Figure 4). Cardiac size and dimensions were generally decreased in the GDF11 group, where significant decreases in left ventricular internal diameter during diastole, posterior wall thickness during systole, and left ventricular mass were apparent by day 10, then later in posterior wall thickness during diastole by day 13 (Figures 4A, 4B, and 4C). GDF11 overexpression also significantly decreased stroke volume (Figure 4D), ejection fraction (Figure 4E), and fractional shortening (Figure 4F) by day 10, compared to control. The echocardiographic measurements of normal and control mice were generally similar, other than an unexplained increase in left ventricular internal diameter in the control mice by day 10 (Figure S2).

Electrocardiography was also performed to further characterize cardiac rate and conductivity following GDF11 exposure; no appreciable differences were observed either when compared to normal or control mice (Figure S3).

Regulatory Pathways in Hearts of Mice with GDF11 Overexpression Demonstrate Increased Degradation of Cardiac Muscle

Western blot analyses of cardiac muscle were performed to detect levels of various mediators in muscle metabolic pathways. GDF11 overexpression increased SMAD2 by day 13. Phosphorylated SMAD2 appeared increased but this did not reach

statistical significance following GDF11 exposure (Figure 5A). Ubiquitin levels were increased in GDF11 mice compared to the control group (Figure 5B). There were no statistically significant differences detected in levels of pFOXO3a, FOXO3a, p4E-BP1, and p62 (Figure S4).

Skeletal Muscle Mass Decreases with GDF11 Overexpression

To examine the effects of GDF11 overexpression on mouse skeletal muscle, we first measured the weights of the left hind limb gastrocnemius, quadriceps, and tibialis muscles. By day 13 after injection with CHO-GDF11 cells, muscle mass was significantly decreased compared to control (Figures 6A, 6B, and 6C). Consistent with this finding, grip strength in the GDF11 mice was also significantly decreased at day 13 (Figure 6D), although a recent study showed improved exercise endurance and grip strength in 33- to 39-month old mice treated with recombinant GDF11 (Sinha et al., 2014). It is interesting to note, however, that myocyte fiber size did not differ significantly between the groups (Figures 6E and 6F). Laminin staining of tibialis muscle cross-sections show myocyte size and shape (Figure 6G).

Gene Markers in Quadriceps of Mice with GDF11 Overexpression Demonstrate Muscle Atrophy

Similar to the GDF11 mouse hearts, the quadriceps of GDF11 mice also indicated a pattern of muscle atrophy. There was significantly increased expression of *atrogin-1* and *MuRF1* by day 13 compared to controls (Figure 6H). *Mki67* expression was significantly decreased and *Bnip3* expression trended towards being increased in the GDF11 group, although there did not appear to be a difference in *Bnip3L* expression (Figure 6H). *Pax7* expression in the muscle was unchanged between GDF11 mice and controls, however, suggesting that GDF11 may not affect muscle regenerative processes differently than controls (Figure 6H).

Increased Degradation and Decreased Synthesis of Skeletal Muscle in Quadriceps of Mice with GDF11 Overexpression

Western blot analyses were also performed on mouse quadriceps. Increased levels of pSMAD2 indicate activation of the GDF11 signaling pathway in mice with GDF11 overexpression. SMAD2 levels were unchanged between GDF11 mice and control, and there was a decrease compared to normal mice (Figure 7A). Levels of mediators of the hypertrophy/atrophy pathway, AKT and FOXO3a, were unchanged with GDF11 overexpression (Figure 7B). FOXO1 was undetected on Western blot. However, GDF11 did affect translational regulation of protein synthesis. Phosphorylated 4E-BP1 levels were decreased in GDF11 mice while 4E-BP1 levels were increased, indicating decreased synthesis of protein in the quadriceps muscle (Figure 7C). Furthermore, increased levels of autophagy markers LC3-II, LC3-II/LC3-I, and p62 (Figure 7D) as well as increased ubiquitin levels (Figure 7E) indicated increased degradation of the skeletal muscle.

CONCLUSION

Our results show that GDF11 overexpression in adult mice leads to cachexia, with consequential cardiac and skeletal muscle dysfunction and weakness. These results are not surprising, as myostatin is 90% homologous to GDF11 and known to be an important player in cachexia (Zimmers et al., 2002). Initial studies (Loffredo et al., 2013; Sinha et al., 2014) showed that GDF11 declines with age, and that the reintroduction of this "factor of youth" (Andersen and Lim, 2014) reverses age-related degenerative changes in the body, such as cardiac hypertrophy and skeletal muscle dysfunction/atrophy (Loffredo et al., 2013; Poggioli et al., 2016; Sinha et al., 2014). In *in vivo* experiments detailed by Smith et al's recent publication, however, they saw no changes in cardiac structure or function with GDF11 administration (Smith et al., 2015). Based on our results, we believe that the previous finding of cardiac hypertrophy reversal with GDF11 administration is not actually a reversion to normal cardiac muscle, but rather atrophy to dysfunctional muscle seen in cachexia. Similarly, we also find that GDF11 overexpression leads to skeletal muscle cachexia.

There are conflicting research findings on body composition changes after GDF11 administration. Poggioli et al's study briefly mentioned observing weight loss in both young and old mice that were given certain doses of exogenous GDF11 (0.5 mg/kg/day and/or 1 mg/kg/day), but this finding was not explored in more detail (Poggioli et al., 2016). At the 0.1 mg/kg/day dosage in Sinha and Jang et al's study, body weight and muscle mass (tibialis and extensor digitorum longus) were shown to be unchanged in both young and old mice in (Sinha et al., 2014). We find that after 13 days of overexpression of GDF11 via CHO cell tumors, body weight decreased dramatically compared to controls, largely contributed by the loss in lean mass. Muscle mass, as measured from the gastrocnemius, quadriceps, and tibialis muscles, also significantly decreased with GDF11 overexpression. The differences in body weight and muscle

mass changes between our study and that of Sinha and Jang et al could potentially be attributed to differences in circulating GDF11 levels.

There have also been conflicting findings on changes in the heart with GDF11 administration. In the Loffredo et al study, intraperitoneal GDF11 administration resulted in decreased heart weight and decreased cardiomyocyte fiber size, but no difference in echocardiography compared to controls (Loffredo et al., 2013). Similarly, Poggioli et al showed that for both young and old mice, intraperitoneal GDF11 administration decreased heart weight as well as cross-sectional area of cardiomyocytes (Poggioli et al., 2016). However, in the Smith et al study, intraperitoneal GDF11 administration in 24 month old mice resulted in no differences in heart weight, echocardiography, terminal hemodynamic studies, cardiomyocyte cross-sectional area, or amount of fibrosis compared to controls (Smith et al., 2015). Our study supports that GDF11 actually promotes cardiac *atrophy* with corresponding decreases in *both* heart size and function. It is interesting to note, however, that a study by Usui et al reported that atrogin-1 mediates cardiac hypertrophy (Usui et al., 2011), contrary to our findings.

In one study of failing hearts (presumably with a hypertrophic component), the investigators found that ANP levels are greater while αMHC and βMHC levels are decreased compared to non-failing hearts (Razeghi et al., 2001). In another study, however, cardiac hypertrophy due to pressure overload was found to increase both αMHC and βMHC levels in cardiomyocytes (Lopez et al., 2011). While these studies differed in the direction of change in the cardiac markers, they nevertheless demonstrated that the levels of cardiac markers are changed by hypertrophic cardiac pathology. In accordance with one of the recent GDF11 studies (Smith et al., 2015), we also found no differences in levels of cardiac markers (ANP, BNP, αMHC, and βMHC) that would suggest pathologic hypertrophy. These findings further support that the

atrophic effects of GDF11 likely do not act by diminishing pathologic cardiac hypertrophy.

Regarding skeletal muscle regenerative potential, Sinha and Jang et al showed that GDF11 supplementation in old mice increased the frequency and function of satellite cells as well as improved exercise endurance and grip strength (Sinha et al., 2014). Conversely, Egerman et al showed that GDF11 treatment did not affect regenerative capacity or cross-sectional area of skeletal muscle after injury; in fact, *in vitro* studies showed that GDF11 actually decreased the growth of adult and aged satellite cells and did not change the expression of markers of muscle differentiation (Egerman et al., 2015). Our studies show that GDF11 overexpression resulted in activation of muscle atrophy pathways, with indications of increased degradation and decreased synthesis of skeletal muscle proteins. Accordingly, the grip strength measurements in our study demonstrated significantly decreased function in GDF11 mice, although we did not study the effects in old mice using our model of CHO cell overexpression. It therefore seems highly unlikely that any regenerative activity seen with satellite cell activation, if present, would result in improved muscle function. In fact, our study shows 20-30% decreases in skeletal muscle mass with GDF11 overexpression while mean cross-sectional area of myocytes is unchanged compared to controls. One possible explanation to these findings is that skeletal myocyte fibers in the GDF11 mice are dying even though the surviving fibers are maintaining their cross-sectional areas, suggesting lack of regenerative potential.

While this study provides another piece of evidence to the GDF11 story, it has its limitations. Unlike other recent *in vivo* investigations of exogenous GDF11 administration in mice, our study used only 10-week old (young) mice. We therefore did not examine the effects of GDF11 overexpression in aged mice (e.g. 24-month old) compared to young mice and cannot say with certainty that our results will also translate with age and

its accompanying physiologic changes. The focus of this study, however, was not so much on how GDF11 overexpression differs with age, but rather on better defining its effects on cardiac and skeletal muscle. Certainly, future studies may be warranted to explore what role, if any, that age plays in changing the pattern of cachexia in those with supraphysiologic levels of GDF11.

This study also did not quantify the exact levels of circulating GDF11 for each mouse. However, we assumed that there were similar amounts of GDF11 expressed and circulating in each experimental mouse, since the same numbers of CHO-GDF11 cells were injected per mouse. We also closely monitored the size of the tumors that grew in the CHO-injected mice, and we discarded the data from an outlier mouse from the GDF11 group that did not have adequate, similar-sized tumor growth compared to the other mice in the same group. Furthermore, we documented induction of GDF11 signaling in the GDF11 mice, observing that phosphorylated SMAD2 levels were increased compared to normal and control mice. Because this study used an overexpression model, however, we were unable to examine the effects of GDF11 at differing lower levels.

We conclude that GDF11 overexpression in adult mice causes significant weight loss and cachexia, specifically causing cardiac and skeletal muscle dysfunction and weakness. Any endeavors to utilize GDF11 as a therapeutic agent should be approached with caution.

FIGURE 1

Overall Body Weight and Composition Decrease with GDF11 Overexpression

(A) Final body weights of normal, control, and GDF11 mice at sacrifice, reported as percentages of initial body weight (IBW). Final body weights of normal mice (n=4) taken at day 13 are shown to the left of the dashed vertical line, and those of control and GDF11 mice at day 10 (n=5 and n=8, respectively) and at day 13 (n=5 and n=7, respectively) are compared to the right of the line. Horizontal lines with error bars indicate mean ± SEM. Statistically significant differences are indicated at $p < 0.01$ (**) and $p < 0.0001$ (****).

(B) Fat mass (left panel) and lean mass (right panel) as measured by EchoMRI™ body composition analysis for normal, control, and GDF11 mice at days 9 and 13. Horizontal lines with error bars indicate mean ± SEM. Statistically significant differences are indicated at $p < 0.0001$ (****).

(C) Control (left) and GDF11 (right) mice at sacrifice, juxtaposed to illustrate significant weight loss in GDF11 mice at day 15.

(D) Organs at necropsy in normal, control, and GDF11 mice at day 15. H, heart; K, kidneys; G, gastrocnemius; T, tibialis; Q, quadriceps; S, spleen; L, liver.

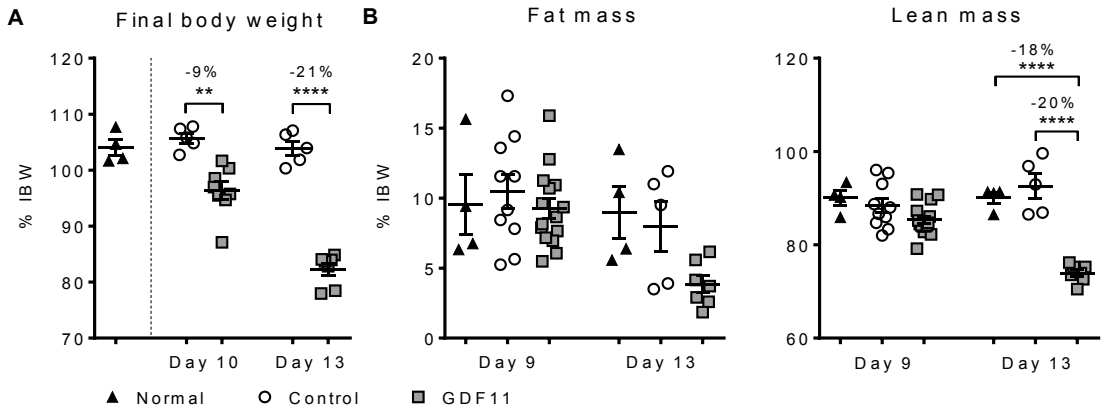
A
Final body weight
% IBW
120
110
100
90
80
70
-9%
**
-21%
****
Day 10
Day 13
Normal
Control
GDF11
B
Fat mass
% IBW
20
15
10
5
0
Day 9
Day 13
Lean mass
120
100
80
60
-18%
****
-20%
****
Day 9
Day 13

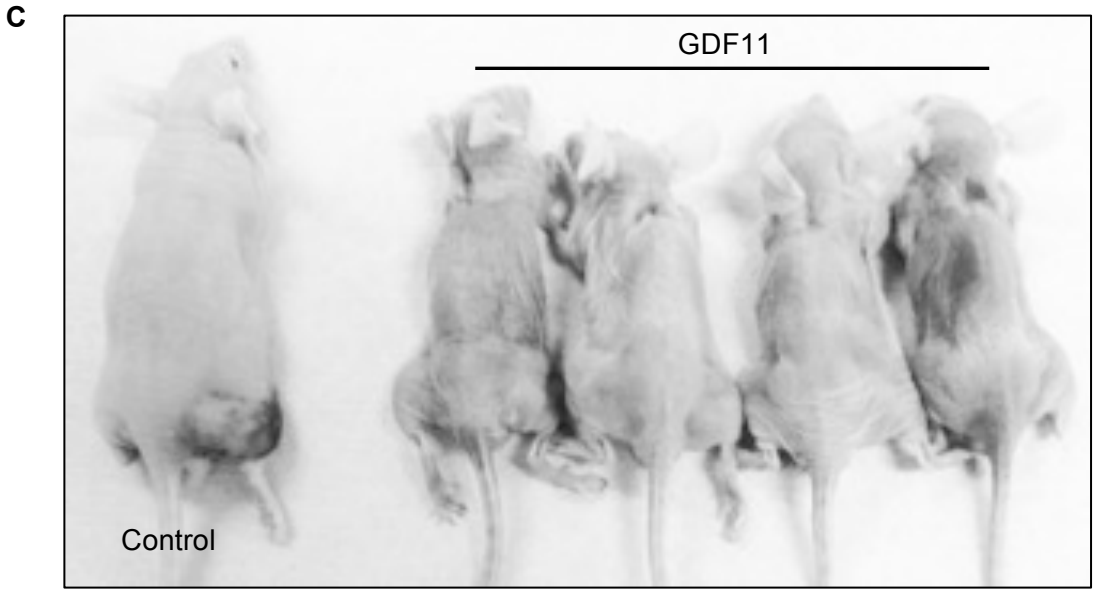
C
GDF11
Control

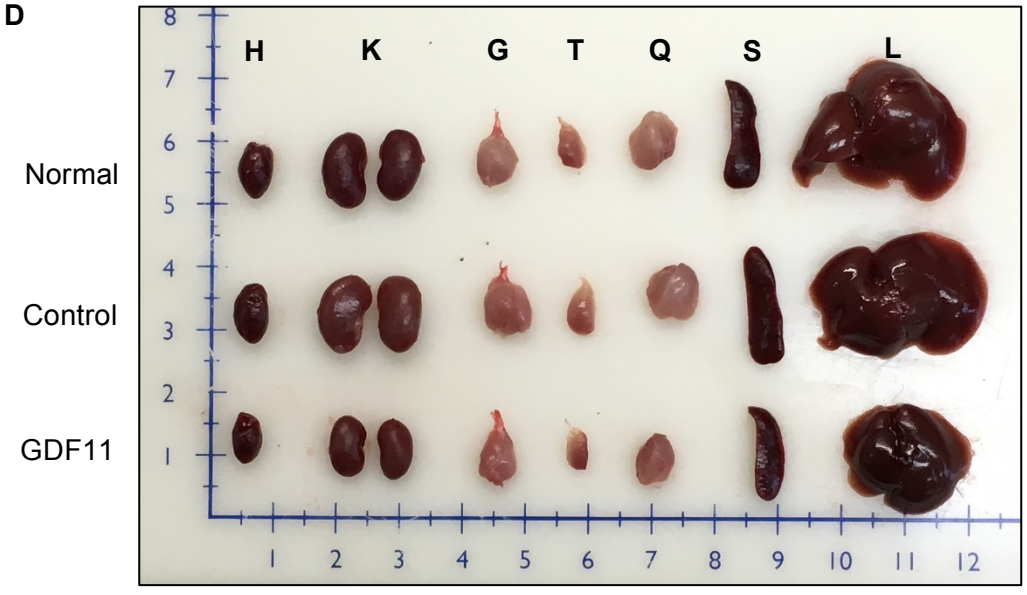
D
H
K
G
T
Q
S
L
Normal
Control
GDF11
1
2
3
4
5
6
7
8
9
10
11
12

FIGURE 2

Heart and Cardiomyocyte Size Decrease with GDF11 Overexpression

(A and B) Heart weights (HW) of normal, control, and GDF11 mice at sacrifice, reported as (A) percentages of initial body weight (IBW) and (B) normalized to tibia length (TL). Heart weights of normal mice (n=4) taken at day 13 are shown to the left of the dashed vertical line, and those of control and GDF11 mice at day 10 (n=5 and n=8, respectively) and at day 13 (n=5 and n=7, respectively) are compared to the right of the line. Horizontal lines with error bars indicate mean ± SEM. Statistically significant differences are indicated at $p < 0.01$ (**) and $p < 0.001$ (***).

(C) Mean cardiomyocyte fiber cross-sectional area (CSA) of normal, control, and GDF11 mice at day 13. Data are mean ± SD. Statistically significant differences are indicated at $p < 0.0001$ (****).

(D) Histogram of cardiomyocyte CSA for normal, control, and GDF11 mice at day 13. Numerical data of mean cardiomyocyte CSA (data are mean ± SEM) and number of fibers measured are shown in table on right.

(E) Gross anatomy (top row of figure on left, 5 mm scale bar) and hematoxylin and eosin staining (cross-section, middle row, 3 mm scale bar; 40x magnification, bottom row) of normal, control, and GDF11 mouse hearts at day 13. LV, left ventricle; RV, right ventricle.

(F) Gene expression analyses of cardiac muscle in normal (left of dashed vertical line, measured at day 13), control, and GDF11 mice at days 10 and 13. Data are represented as mean fold change ± SD. Fold change for *atrogin-1* and *MuRF1* were calculated using reference gene TBP, while data for all other genes were calculated using reference gene 18S. Statistically significant differences are indicated at $p < 0.05$ (*), $p < 0.001$ (***) and $p < 0.0001$ (****).

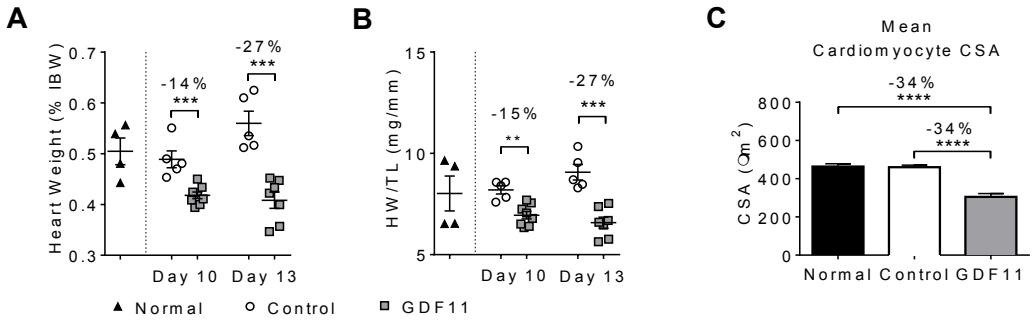

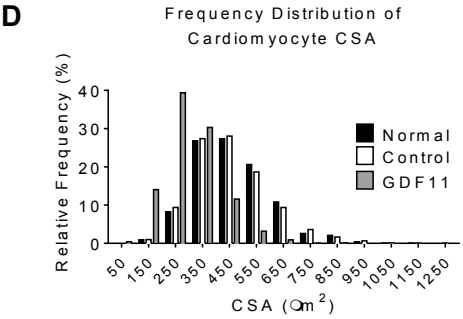

Mean Cardiomyocyte CSA per Group

	CSA (μm²)	Fibers Measured (N)
Normal	465.42 ± 139.03	1480
Control	460.37 ± 143.16	1526
GDF11	303.1 ± 102.82	1729

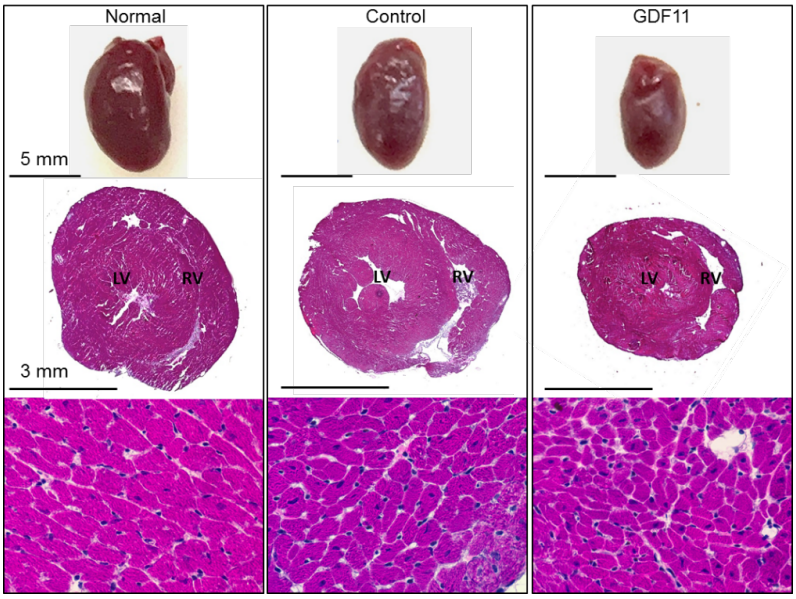

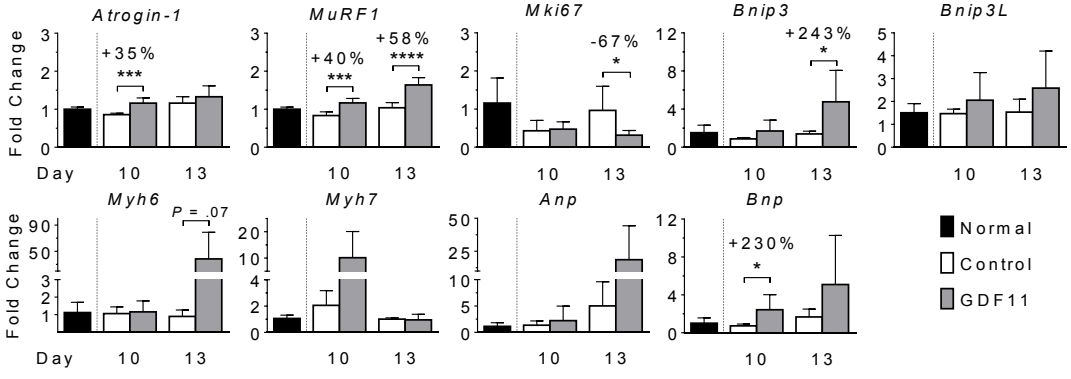

FIGURE 3

Echocardiographic Images in Mice with GDF11 Overexpression Demonstrate Reduced Cardiac Size and Function

(A and B) Brightness mode image views of control and GDF11 mouse hearts in the parasternal (A) long axis view of the left ventricle (outlined in gray) during systole and diastole and the (B) short axis view of the left ventricle at the papillary muscle level during systole, taken at day 13. AW, anterior wall; LV, left ventricle; PM, papillary muscle; PW, posterior wall. White scale bars on bottom left corner, 1 mm.

(C) Motion mode imaging of control and GDF11 mouse hearts for left ventricular wall, chamber, and cardiac function measurements at day 13. LVIDd/s, left ventricular internal diameter (diastole/systole); PW, posterior wall.

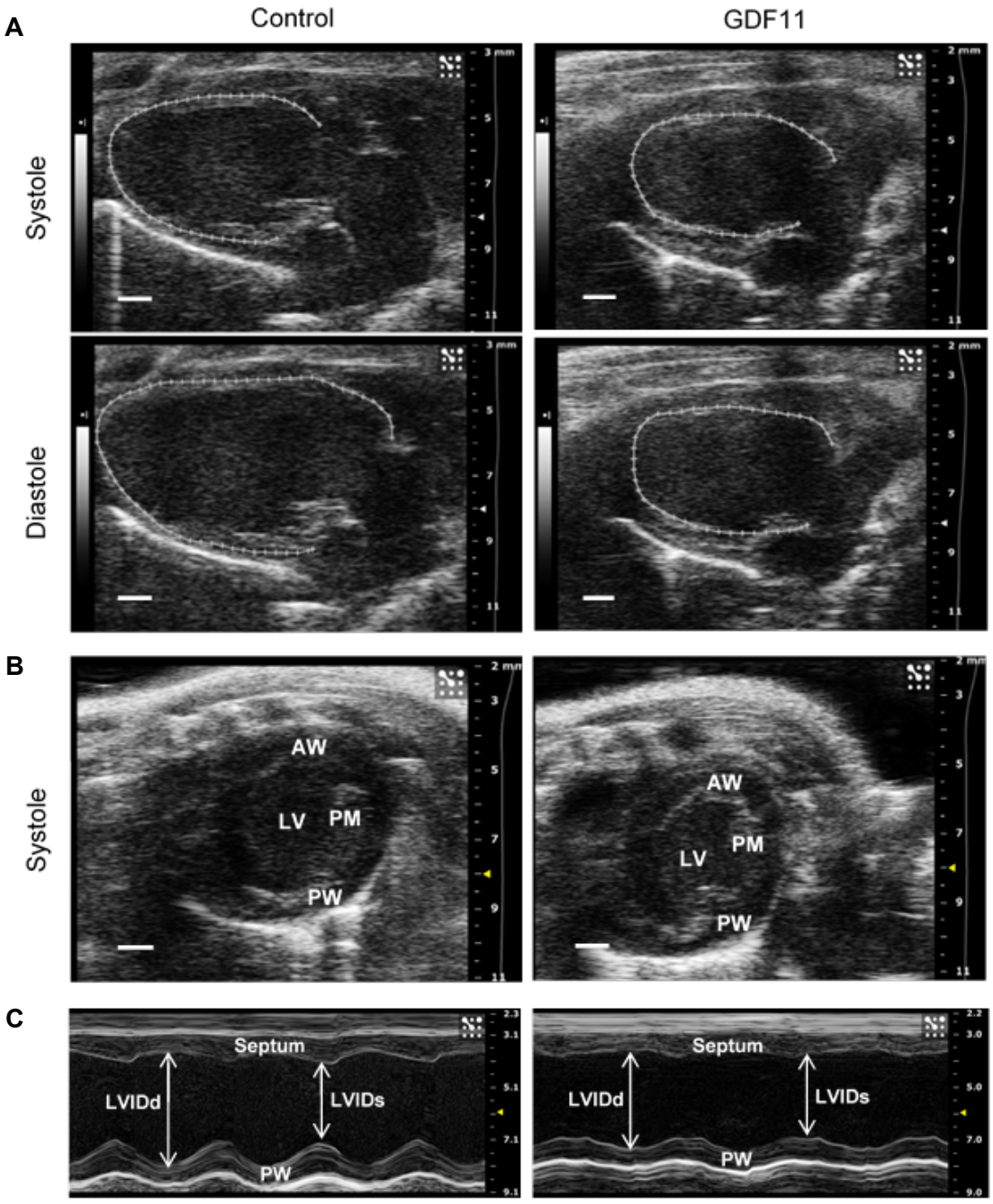
A
Control
GDF11
Systole
Diastole
B
Systole
AW
LV
PM
PW
AW
LV
PM
PW
C
Septum
LVIDd
LVIDs
PW
Septum
LVIDd
LVIDs
PW

FIGURE 4

Echocardiographic Measurements in Mice with GDF11 Overexpression Demonstrate Reduced Cardiac Size and Function

(A and B) Time course of echocardiographic dimension changes in control and GDF11 mice. (A) Left ventricular internal diameter (diastole/systole) (LVIDd/s) and (B) posterior wall thickness (diastole/systole) (PWTd/s) measurements are shown.

(C-F) Time course of changes in echocardiographic measurements of (C) left ventricle (LV) mass and cardiac function as measured by (D) stroke volume, (E) ejection fraction, and (F) fractional shortening. Horizontal lines with error bars indicate mean ± SD. Statistically significant differences are indicated at $p < 0.05$ (*), $p < 0.01$ (**), and $p < 0.001$ (***).

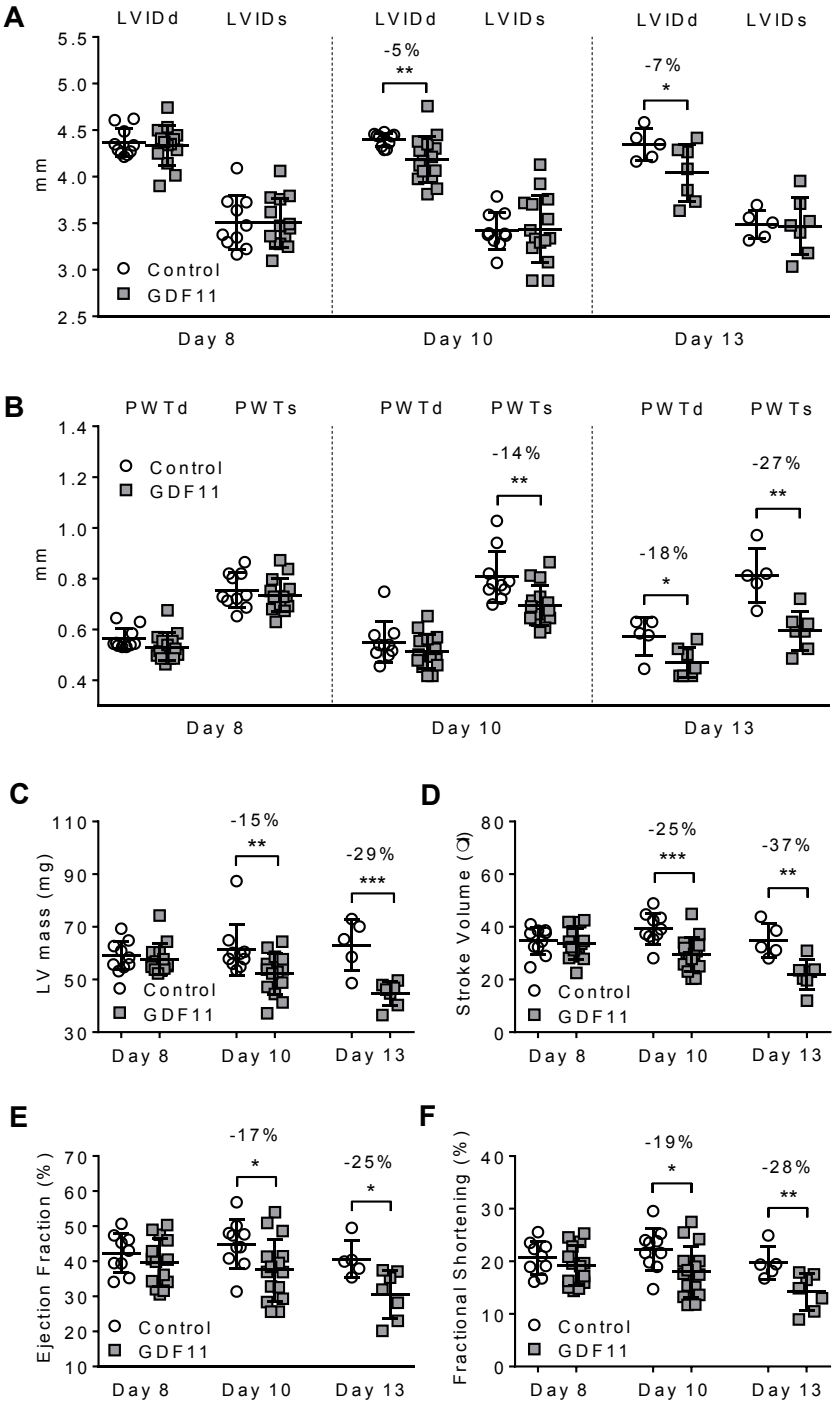
A
LVIDd
LVIDs
LVIDd
LVIDs
LVIDd
LVIDs
-5%
**
-7%
*
mm
5.5
5.0
4.5
4.0
3.5
3.0
2.5
Control
GDF11
Day 8
Day 10
Day 13
B
PWTd
PWTs
PWTd
PWTs
PWTd
PWTs
-14%
**
-18%
*
-27%
**
mm
1.4
1.2
1.0
0.8
0.6
0.4
Control
GDF11
Day 8
Day 10
Day 13
C
LV mass (mg)
110
90
70
50
30
-15%
**
-29%
***
Control
GDF11
Day 8
Day 10
Day 13
D
Stroke Volume (Ml)
80
60
40
20
0
-25%
***
-37%
**
Control
GDF11
Day 8
Day 10
Day 13
E
Ejection Fraction (%)
70
60
50
40
30
20
10
-17%
*
-25%
*
Control
GDF11
Day 8
Day 10
Day 13
F
Fractional Shortening (%)
40
30
20
10
0
-19%
*
-28%
**
Control
GDF11
Day 8
Day 10
Day 13

FIGURE 5

Protein Regulatory Pathways in Hearts of Mice with GDF11 Overexpression Demonstrate Increased Degradation

(A and B) Western blotting analyses to determine (A) activation of SMAD2 signaling and (B) ubiquitination levels in normal, control, and GDF11 mice at day 13. Blots are presented on the top and protein levels quantified in graphs on the bottom. Horizontal lines with error bars indicate mean ± SD. Statistically significant differences are indicated at $p < 0.05$ (*).

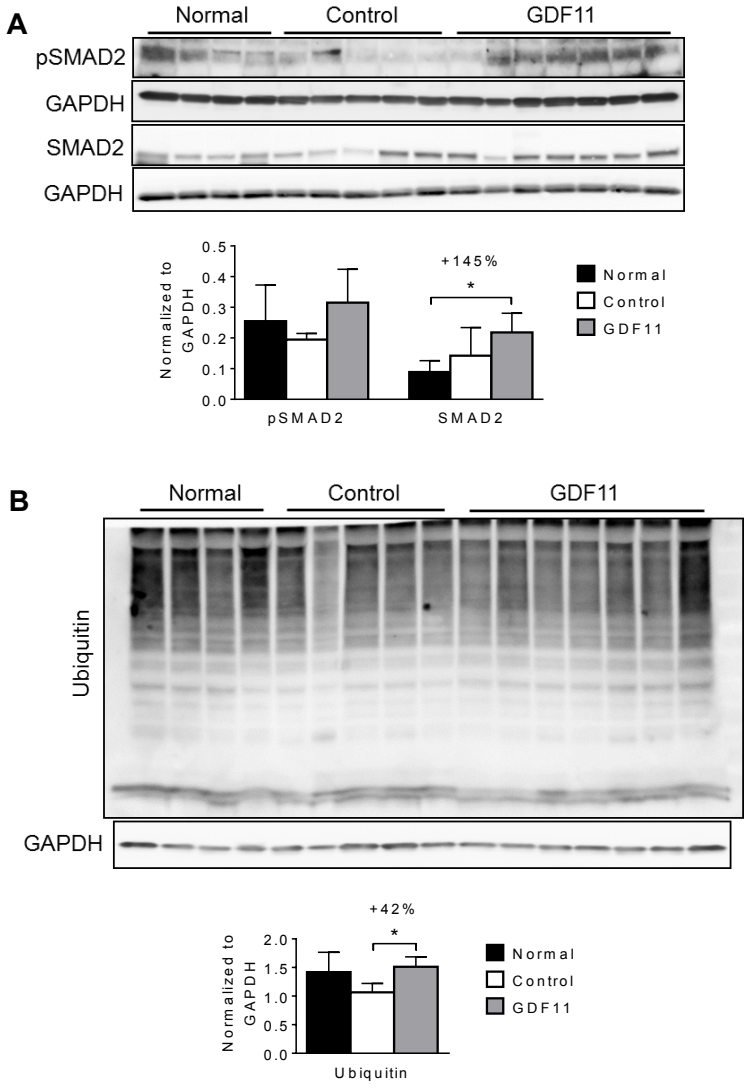

FIGURE 6

Skeletal Muscle Weight and Function Decrease with GDF11 Overexpression

(A-C) Weights of the left hind limb (A) gastrocnemius, (B) quadriceps, and (C) tibialis muscles taken at sacrifice were reported as percentages of initial body weight (IBW). Muscle weights of normal mice (n=4) taken at day 13 are shown to the left of the dashed vertical line, and those of control and GDF11 mice at day 10 (n=5 and n=8, respectively) and at day 13 (n=5 and n=7, respectively) are compared to the right of the line. Horizontal lines with error bars indicate mean ± SEM. Statistically significant differences are indicated at $p < 0.05$ (*), $p < 0.01$ (**), and $p < 0.0001$ (****).

(D) Grip strength measurements at day 10 and 13. Each data point is an average of 3 separate measurements in each mouse. Horizontal lines with error bars indicate mean ± SEM. Statistically significant differences are indicated at $p < 0.05$ (*).

(E) Mean quadriceps myocyte fiber cross-sectional area (CSA) of normal, control, and GDF11 mice at day 13. Data are mean ± SEM.

(F) Histogram of quadriceps CSA for normal, control, and GDF11 mice at day 13.

(G) Laminin staining (10x magnification, 100 μm scale bar) of left hind limb quadriceps muscle cross-sections in normal, control, and GDF11 mice at day 13. Numerical data of mean myocyte CSA (data are mean ± SEM) and number of fibers measured are shown in table below.

(H) Gene expression analyses of quadriceps muscle in normal (left of dashed vertical line, measured at day 13), control, and GDF11 mice at days 10 and 13. Data are represented as mean fold change ± SD. All fold changes calculated using reference gene 18S. Statistically significant differences are indicated at $p < 0.05$ (*) and $p < 0.001$ (***).

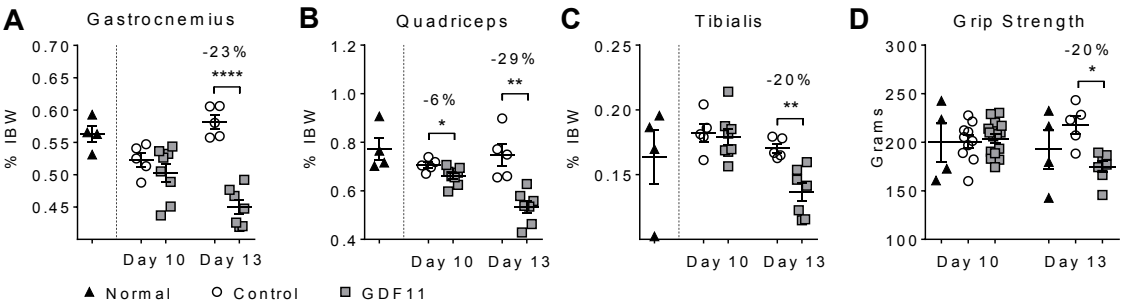

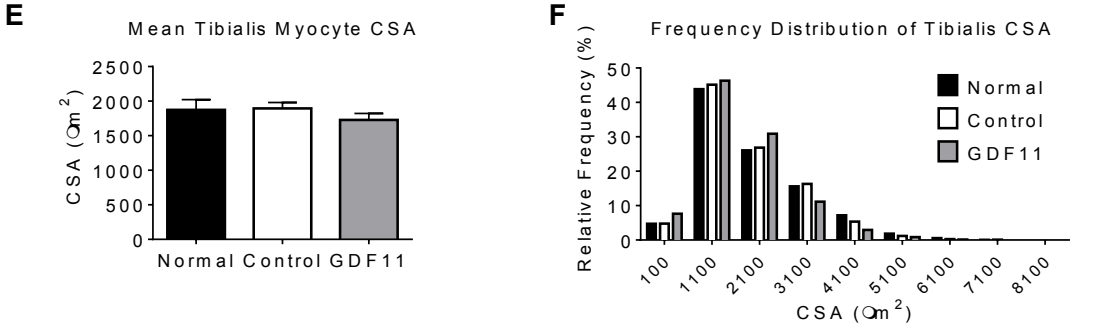

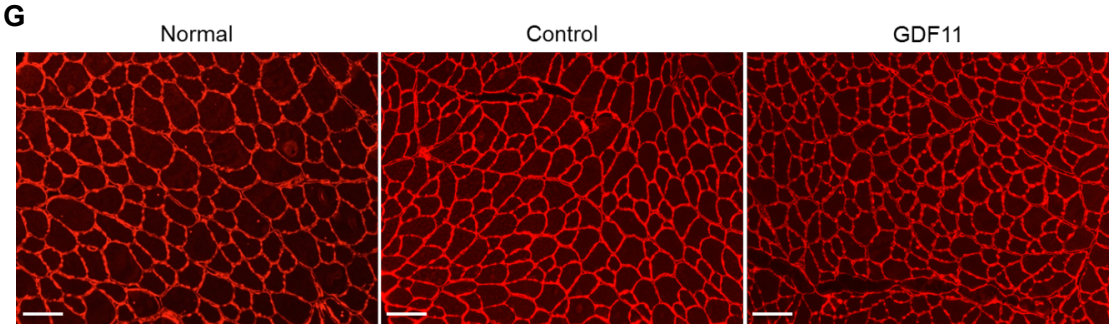

Mean Myocyte CSA per Group

	CSA (μm²)	Fibers Measured (N)
Normal	1874 ± 148.7	3386
Control	1896 ± 85.4	6587
GDF11	1729 ± 94.2	9266

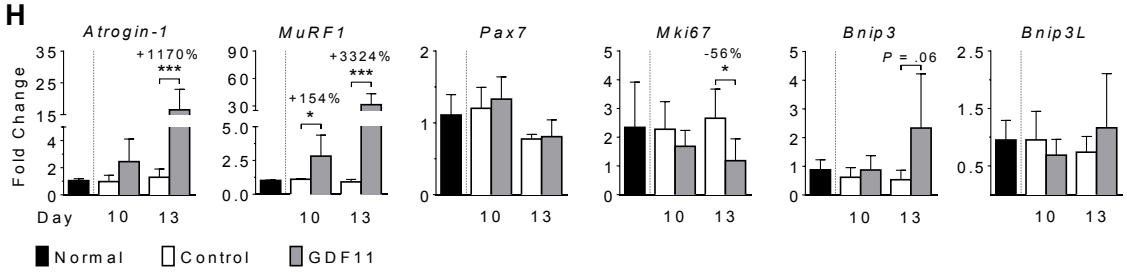

FIGURE 7

Protein Regulatory Pathways in Quadriceps of Mice with GDF11 Overexpression Demonstrate Increased Degradation and Decreased Synthesis

(A-E) Western blotting analyses to determine activation of (A) SMAD2 signaling, (B) hypertrophy/atrophy pathways (arrowhead points to FOXO3a), (C) protein translation and synthesis, (D) autophagy, and (E) ubiquitination in normal, control, and GDF11 mice at day 13. Blots are presented on the top and protein levels quantified in graphs on the bottom. Horizontal lines with error bars indicate mean ± SD. Statistically significant differences are indicated at $p < 0.05$ (*), $p < 0.01$ (**), and $p < 0.0001$ (****).

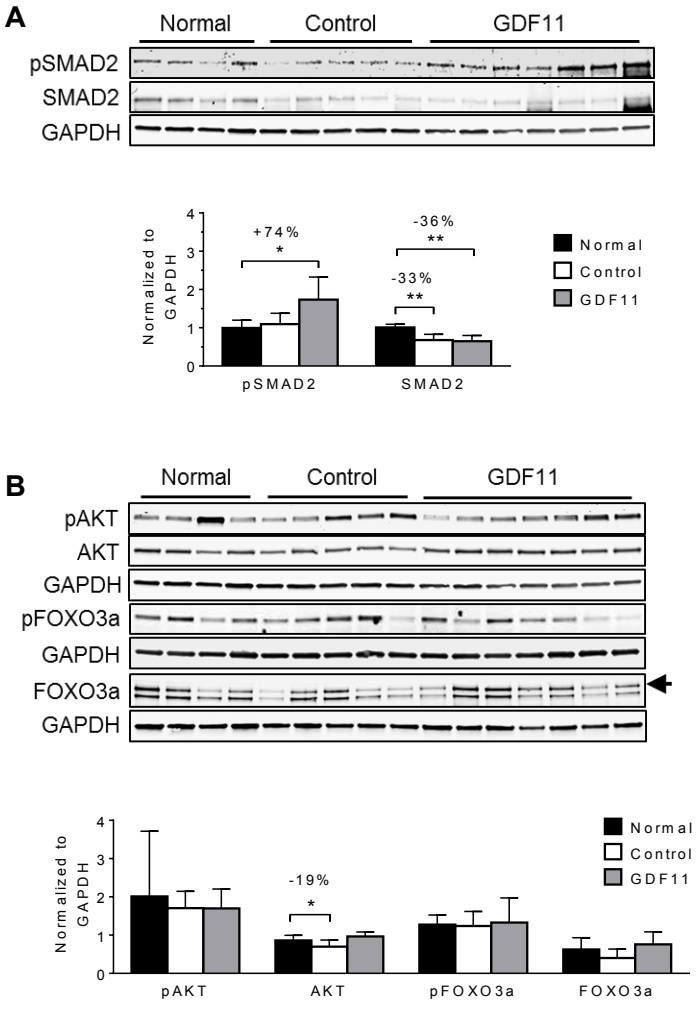

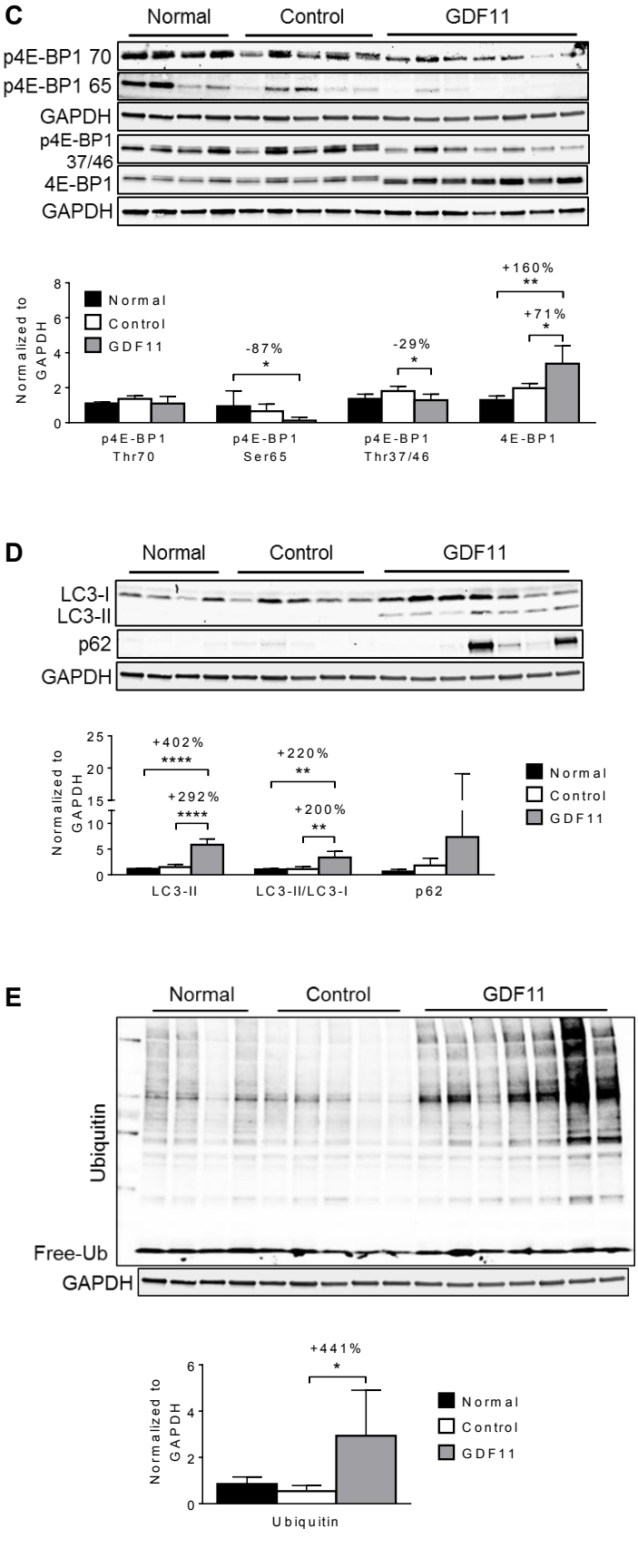
C
Normal
Control
GDF11
p4E-BP1 70
p4E-BP1 65
GAPDH
p4E-BP1 37/46
4E-BP1
GAPDH
Normalized to GAPDH
Normal
Control
GDF11
-87%
*
-29%
*
+160%
**
+71%
*
p4E-BP1 Thr70
p4E-BP1 Ser65
p4E-BP1 Thr37/46
4E-BP1
D
Normal
Control
GDF11
LC3-I
LC3-II
p62
GAPDH
Normalized to GAPDH
+402%
****
+292%
****
+220%
**
+200%
**
Normal
Control
GDF11
LC3-II
LC3-II/LC3-I
p62
E
Normal
Control
GDF11
Ubiquitin
Free-Ub
GAPDH
Normalized to GAPDH
+441%
*
Normal
Control
GDF11
Ubiquitin

FIGURE S1

Reduced Organ Weights in Mice with GDF11 Overexpression

(A-F) Weights of (A) carcasses and (B-F) various organs at sacrifice, reported as percentages of initial body weight (IBW). Final body weights of normal mice (n=4) taken at day 13 are shown to the left of the dashed vertical line, and those of control and GDF11 mice at day 10 (n=5 and n=8, respectively) and at day 13 (n=5 and n=7, respectively) are compared to the right of the line. Horizontal lines with error bars indicate mean ± SEM. Statistically significant differences are indicated at $p < 0.05$ (*), $p < 0.001$ (***), and $p < 0.0001$ (****).

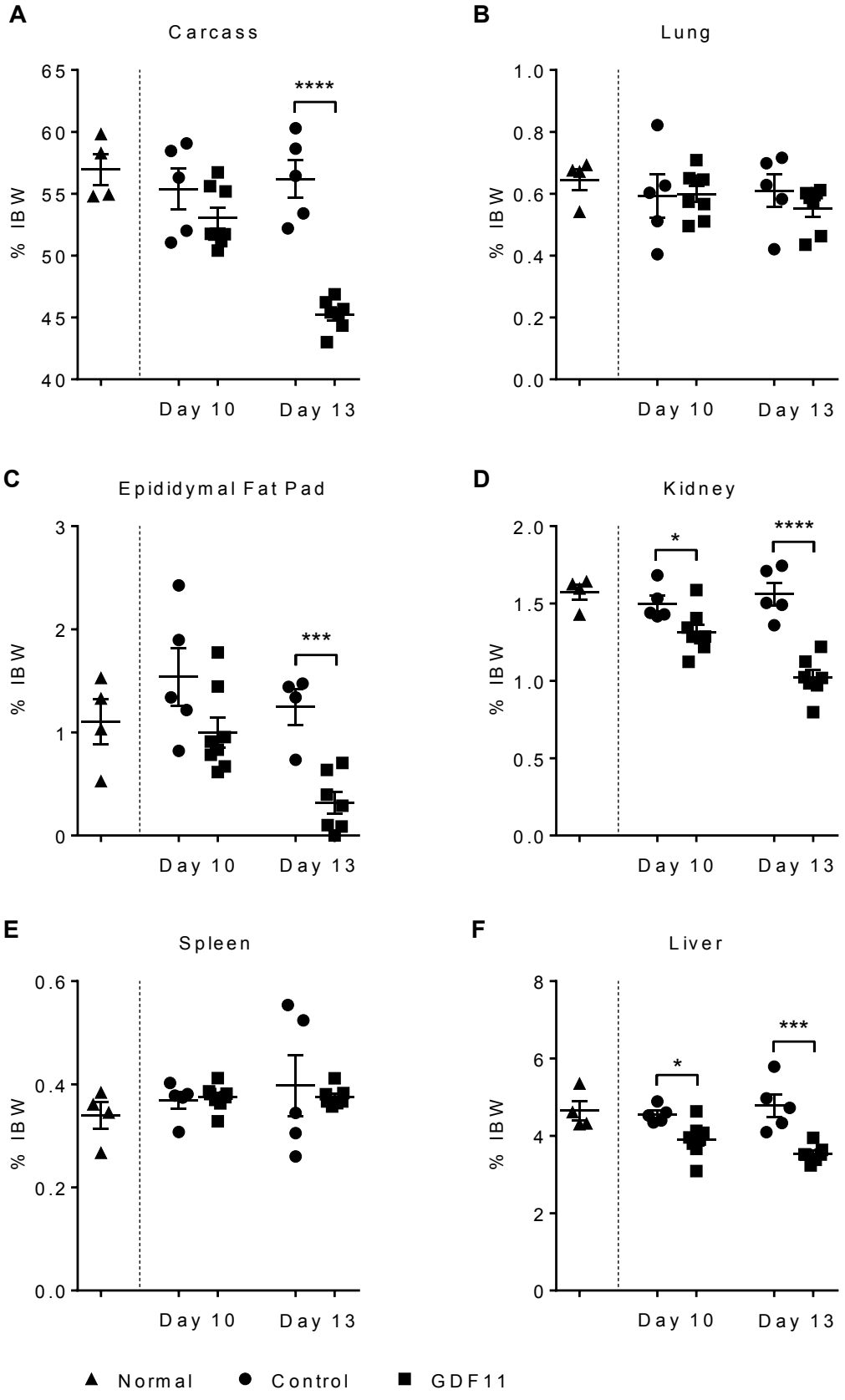
A
Carcass
% IBW
65
60
55
50
45
40
****
Day 10
Day 13
B
Lung
% IBW
1.0
0.8
0.6
0.4
0.2
0.0
Day 10
Day 13
C
Epididymal Fat Pad
% IBW
3
2
1
0
***
Day 10
Day 13
D
Kidney
% IBW
2.0
1.5
1.0
0.5
0.0
*
****
Day 10
Day 13
E
Spleen
% IBW
0.6
0.4
0.2
0.0
Day 10
Day 13
F
Liver
% IBW
8
6
4
2
0
*
***
Day 10
Day 13
Normal
Control
GDF11

FIGURE S2

Echocardiography in Normal and Control Mice are Similar

(A and B) Time course of echocardiographic dimension changes in normal and control mice. (A) Left ventricular internal diameter (diastole/systole) (LVIDd/s) and (B) posterior wall thickness (diastole/systole) (PWTd/s) measurements are shown.

(C-F) Time course of changes in echocardiographic measurements of (C) left ventricle (LV) mass and cardiac function as measured by (D) stroke volume, (E) ejection fraction, and (F) fractional shortening. Horizontal lines with error bars indicate mean ± SD. Statistically significant differences are indicated at $p < 0.05$ (*) and $p < 0.01$ (**).

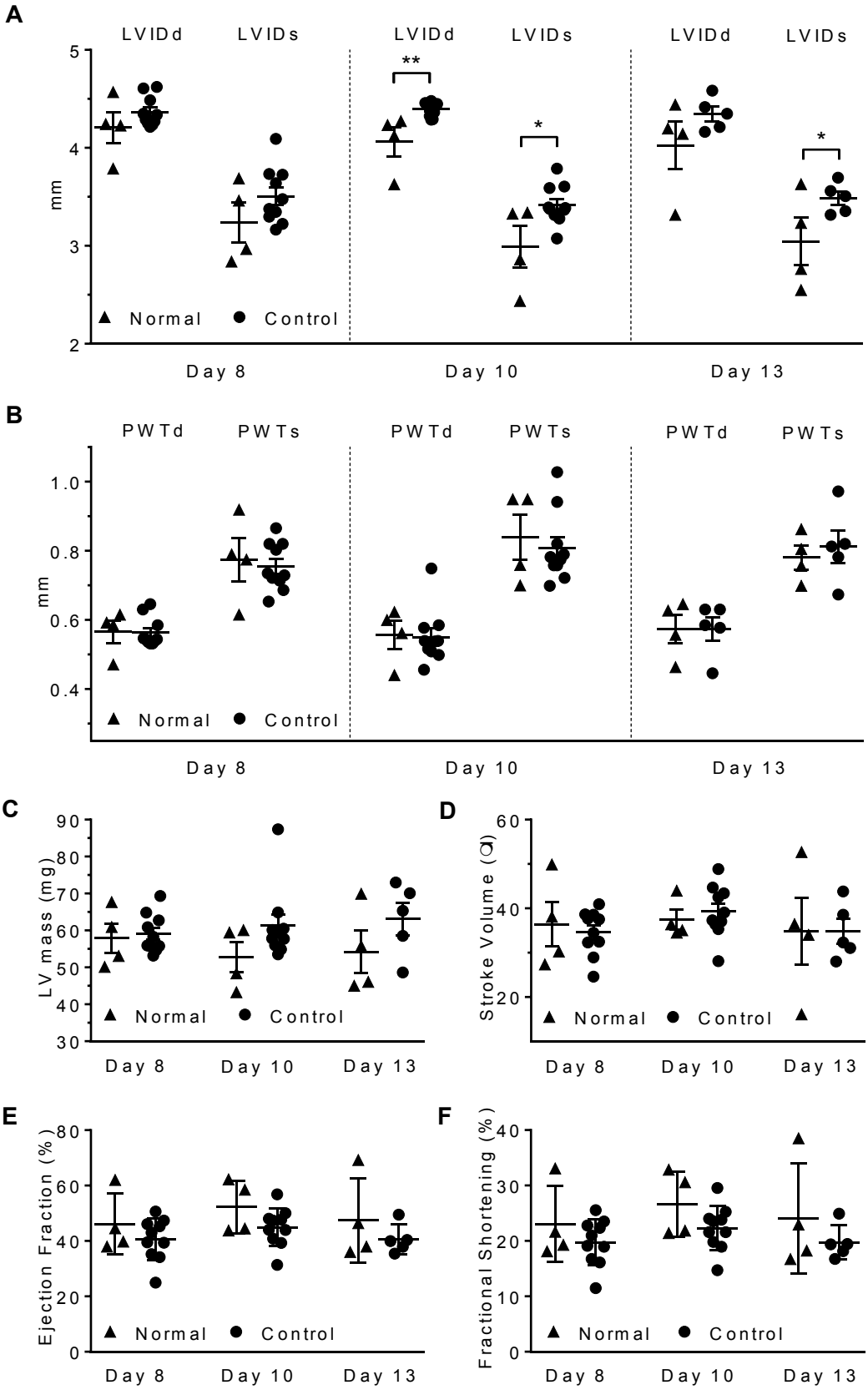
A
LVIDd
LVIDs
LVIDd
LVIDs
LVIDd
LVIDs
5
4
3
2
mm
**
*
*
Normal
Control
Day 8
Day 10
Day 13
B
PWTd
PWTs
PWTd
PWTs
PWTd
PWTs
1.0
0.8
0.6
0.4
mm
Normal
Control
Day 8
Day 10
Day 13
C
LV mass (mg)
90
80
70
60
50
40
30
Normal
Control
Day 8
Day 10
Day 13
D
Stroke Volume (Ql)
60
40
20
Normal
Control
Day 8
Day 10
Day 13
E
Ejection Fraction (%)
80
60
40
20
0
Normal
Control
Day 8
Day 10
Day 13
F
Fractional Shortening (%)
40
30
20
10
0
Normal
Control
Day 8
Day 10
Day 13

FIGURE S3

Electrocardiography is Unchanged in Mice with GDF11 Overexpression

(A-I) Time course of electrocardiographic measurements of normal (n=4), control (n=10, days 7 and 9; n=5, day 13), and GDF11 (n=16, days 7 and 9; n=8, day 13) mice. Data points represent mean ± SD. Statistically significant difference is indicated at $p < 0.05$ (*).

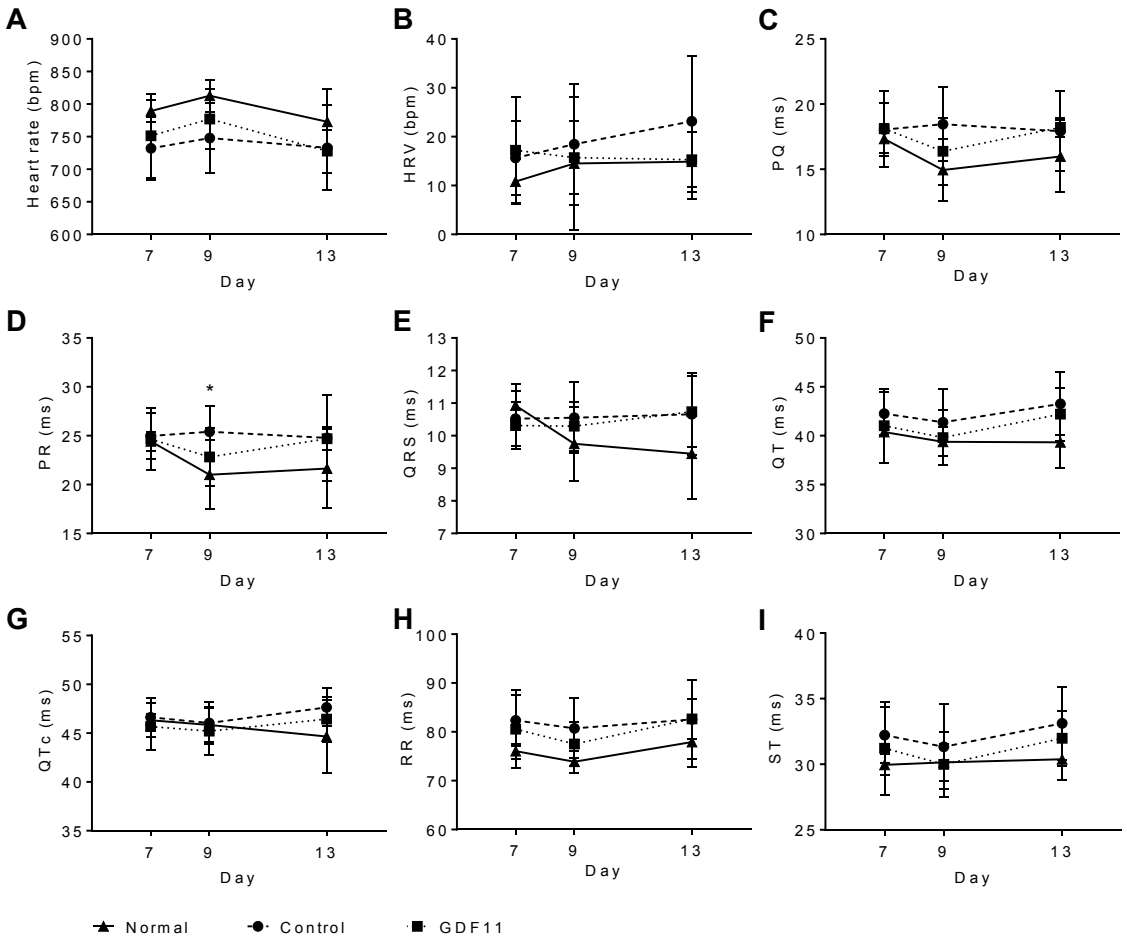

FIGURE S4

Protein Expression in Hearts of Mice with GDF11 Overexpression

(A-C) Western blotting analyses to determine activation of (A) hypertrophy/atrophy pathways, (B) protein translation and synthesis, and (C) autophagy in normal, control, and GDF11 mice at day 13. Blots are presented on the top and protein levels quantified in graphs on the bottom. Horizontal lines with error bars indicate mean ± SD.

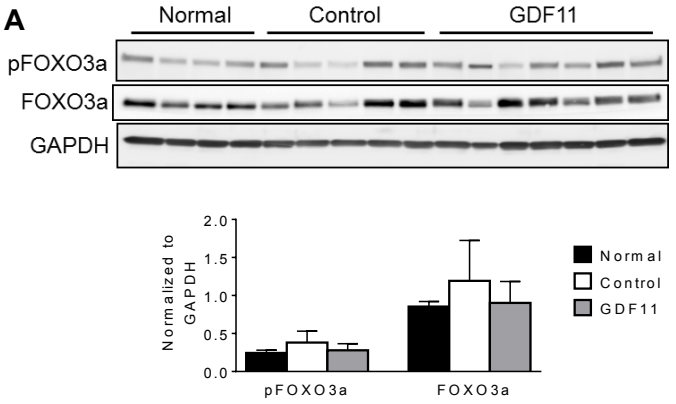

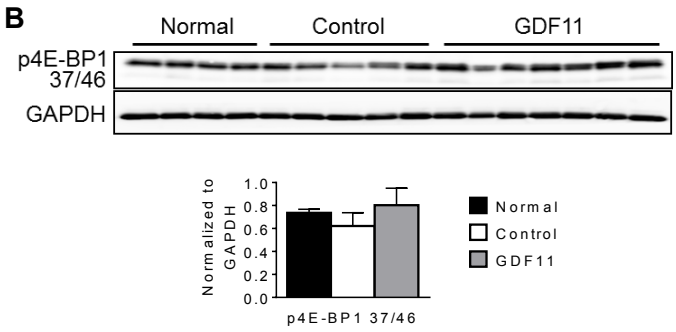

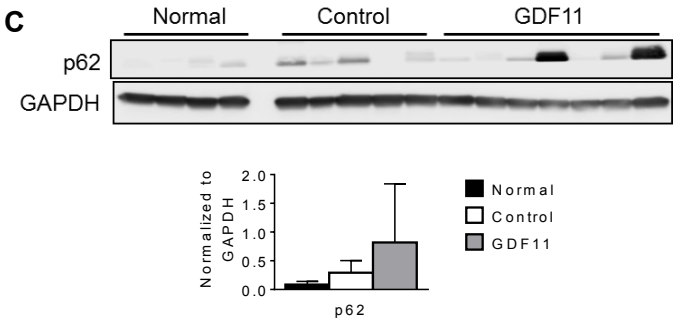

REFERENCES

Andersen, R.E., and Lim, D.A. (2014). An ingredient for the elixir of youth. Cell Res *24*, 1381-1382.

Bodine, S.C., Latres, E., Baumhueter, S., Lai, V.K., Nunez, L., Clarke, B.A., Poueymirou, W.T., Panaro, F.J., Na, E., Dharmarajan, K., et al. (2001). Identification of ubiquitin ligases required for skeletal muscle atrophy. Science (New York, N.Y.) *294*, 1704-1708.

Bonetto, A., Aydogdu, T., Jin, X., Zhang, Z., Zhan, R., Puzis, L., Koniaris, L.G., and Zimmers, T.A. (2012). JAK/STAT3 pathway inhibition blocks skeletal muscle wasting downstream of IL-6 and in experimental cancer cachexia. American journal of physiology. Endocrinology and metabolism *303*, E410-421.

Egerman, M.A., Cadena, S.M., Gilbert, J.A., Meyer, A., Nelson, H.N., Swalley, S.E., Mallozzi, C., Jacobi, C., Jennings, L.L., Clay, I., et al. (2015). GDF11 Increases with Age and Inhibits Skeletal Muscle Regeneration. Cell metabolism *22*, 164-174.

Gomes, M.D., Lecker, S.H., Jagoe, R.T., Navon, A., and Goldberg, A.L. (2001). Atrogin-1, a muscle-specific F-box protein highly expressed during muscle atrophy. Proceedings of the National Academy of Sciences of the United States of America *98*, 14440-14445.

Jin, X., Zhang, Z., Beer-Stolz, D., Zimmers, T.A., and Koniaris, L.G. (2007). Interleukin-6 inhibits oxidative injury and necrosis after extreme liver resection. Hepatology (Baltimore, Md.) *46*, 802-812.

Jin, X., Zimmers, T.A., Perez, E.A., Pierce, R.H., Zhang, Z., and Koniaris, L.G. (2006). Paradoxical effects of short- and long-term interleukin-6 exposure on liver injury and repair. Hepatology (Baltimore, Md.) *43*, 474-484.

Loffredo, F.S., Steinhauser, M.L., Jay, S.M., Gannon, J., Pancoast, J.R., Yalamanchi, P., Sinha, M., Dall'Osso, C., Khong, D., Shadrach, J.L., et al. (2013). Growth differentiation factor 11 is a circulating factor that reverses age-related cardiac hypertrophy. Cell *153*, 828-839.

Lopez, J.E., Myagmar, B.E., Swigart, P.M., Montgomery, M.D., Haynam, S., Bigos, M., Rodrigo, M.C., and Simpson, P.C. (2011). beta-myosin heavy chain is induced by pressure overload in a minor subpopulation of smaller mouse cardiac myocytes. Circulation research *109*, 629-638.

McPherron, A.C., Lawler, A.M., and Lee, S.J. (1999). Regulation of anterior/posterior patterning of the axial skeleton by growth/differentiation factor 11. Nature genetics *22*, 260-264.

Mielcarek, M., Inuabasi, L., Bondulich, M.K., Muller, T., Osborne, G.F., Franklin, S.A., Smith, D.L., Neueder, A., Rosinski, J., Rattray, I., et al. (2014). Dysfunction of the CNS-heart axis in mouse models of Huntington's disease. PLoS genetics *10*, e1004550.

Nakashima, M., Toyono, T., Akamine, A., and Joyner, A. (1999). Expression of growth/differentiation factor 11, a new member of the BMP/TGFbeta superfamily during mouse embryogenesis. Mechanisms of development *80*, 185-189.

Poggioli, T., Vujic, A., Yang, P., Macias-Trevino, C., Uygur, A., Loffredo, F.S., Pancoast, J.R., Cho, M., Goldstein, J., Tandias, R.M., et al. (2016). Circulating Growth Differentiation Factor 11/8 Levels Decline With Age. Circulation research *118*, 29-37.

Razeghi, P., Young, M.E., Alcorn, J.L., Moravec, C.S., Frazier, O.H., and Taegtmeyer, H. (2001). Metabolic gene expression in fetal and failing human heart. Circulation *104*, 2923-2931.

Rodgers, B.D., and Eldridge, J.A. (2015). Reduced Circulating GDF11 Is Unlikely Responsible for Age-Dependent Changes in Mouse Heart, Muscle, and Brain. Endocrinology *156*, 3885-3888.

Sinha, M., Jang, Y.C., Oh, J., Khong, D., Wu, E.Y., Manohar, R., Miller, C., Regalado, S.G., Loffredo, F.S., Pancoast, J.R., et al. (2014). Restoring systemic GDF11 levels reverses age-related dysfunction in mouse skeletal muscle. Science (New York, N.Y.) *344*, 649-652.

Smith, S.C., Zhang, X., Zhang, X., Gross, P., Starosta, T., Mohsin, S., Franti, M., Gupta, P., Hayes, D., Myzithras, M., et al. (2015). GDF11 Does Not Rescue Aging-Related Pathological Hypertrophy. Circulation research.

Usui, S., Maejima, Y., Pain, J., Hong, C., Cho, J., Park, J.Y., Zablocki, D., Tian, B., Glass, D.J., and Sadoshima, J. (2011). Endogenous muscle atrophy F-box mediates pressure overload-induced cardiac hypertrophy through regulation of nuclear factor-kappaB. Circulation research *109*, 161-171.

Zimmers, T.A., Davies, M.V., Koniaris, L.G., Haynes, P., Esquela, A.F., Tomkinson, K.N., McPherron, A.C., Wolfman, N.M., and Lee, S.J. (2002). Induction of cachexia in mice by systemically administered myostatin. Science (New York, N.Y.) *296*, 1486-1488.

Zimmers, T.A., McKillop, I.H., Pierce, R.H., Yoo, J.Y., and Koniaris, L.G. (2003). Massive liver growth in mice induced by systemic interleukin 6 administration. Hepatology (Baltimore, Md.) *38*, 326-334.

CURRICULUM VITAE

Tiffany Liang

Education

Master of Science in Translational Science
IUPUI, Indianapolis, IN (August 2016)

Doctor of Medicine
Medical College of Georgia, Augusta, GA (May 2012)

Bachelor of Science in Engineering Degree, Biomedical Engineering, with Distinction
Duke University, Durham, NC (May 2008)

Professional Experience

General Surgery Resident, 2012 – current
Indiana University Health, Indianapolis, IN

Research and Training Experience

Cardiac and skeletal muscle atrophy with GDF11 overexpression
Department of Surgery, Indiana University School of Medicine, Indianapolis, IN (2015 – current)
Principle Investigators: Dr. Teresa A. Zimmers, Dr. Leonidas G. Koniaris

Autoimmunity in abdominal aortic aneurysms
Department of Medicine, Indiana University School of Medicine, Indianapolis, IN (2014 – 2015)
Principle Investigator: Dr. David S. Wilkes

Publications

Chang TW, Gracon A, Murphy MP, Wilkes DS. Exploring autoimmunity in the pathogenesis of abdominal aortic aneurysms. *Am J Physiol Heart Circ Physiol.* 2015 Sep;309(5):H719-27. doi: 10.1152/ajpheart.00273.2015.

Liang TW, Jester A, Motaganahalli RL, Wilson MG, G'Sell P, Akingba GA, Fajardo A, Murphy MP. Autologous bone marrow mononuclear cell therapy for critical limb ischemia is effective and durable. *J Vasc Surg*. 2016 Mar 23. pii: S0741-5214(16)00133-6. doi: 10.1016/j.jvs.2016.01.022.

Liang TW, Gracon A, Rothhaar K, Wu J, Wilkes DS. HLA-DR13, DR15 are associated with short-term lung transplant outcomes. *J Surg Res*. Accepted on March 18, 2016. Article in press.

Lemmon GW, Motaganahalli RL, **Chang T**, Slaven J, Aumiller B, Kim BJ, Dalsing MC. Failure mode analysis of the Endologix endograft. *J Vasc Surg*. 2016 May 14. pii: S0741-5214(16)00829-6. doi: 10.1016/j.jvs.2016.03.416.

Kim BJ, Valsangkar NP, **Liang TW**, Murphy MP, Zimmers TA, Bell TM, Davies M, Koniaris LG. Impact of integrated vascular residencies on academic productivity within vascular surgery divisions. Article in press at *Ann Vasc Surg*.

Gracon A, **Liang TW**, Easterday TS, Weber DJ, Butler J, Slaven JE, Lemmon GW, Motaganahalli RL. Institutional cost of unplanned 30 day readmission following open and endovascular surgery. Manuscript currently under revision at *Vasc Endovascular Surg.*

Valsangkar NP, **Liang TW**, Martin PJ, Mayo JS, Rosati CM, Feliciano DV, Zimmers TA, Koniaris LG. The impact of clinical fellowships on academic productivity in departments of surgery. Manuscript currently under revision at *Surgery*.

Gracon A, **Liang TW**, Rothhaar K, Zaffiri L, Wu J, Pandya P, Wilkes DS. The impact of the donor cause of brain death and duration of brain death on survival and bronchiolitis obliterans syndrome post lung transplantation. Manuscript to be submitted to *Am J Transplantation.*

Liang TW, Feliciano DV, Koniaris LG. A surgery trainee's guide to writing a manuscript. Manuscript currently under revision for *Bull Am Coll Surg.*

Conferences Attended

Liang TW. (2016). HLA-DR13 and -DR15 Are Associated with Short-term Rejection in Lung Transplantation. Paper presented at the 11th Annual Academic Surgical Congress, Jacksonville, FL.

Chang TW. (2015). Institutional cost of unplanned 30-day readmission following open and endovascular surgery. Paper presented at the annual meeting of the South Asian Association for Vascular Surgery, Chicago, IL.

Honors, Awards, Fellowships

South Asian Association for Vascular Surgery 2015 Research Abstract Competition Award (2015)
Society of Vascular Surgery Vascular 2015 Annual Meeting Resident Travel Scholarship (2015)
Medical College of Georgia Dean's Summer Research Fellow (2009)
Howard G. Clark Award (2008)
Duke University Pratt Undergraduate Research Fellow (2007-2008)
Duke University Pratt School of Engineering Dean's List (2005-2007)

THE END